ISSN 0915-633

NATIONAL INSTITUTE FOR FUSION SCIENCE

Application of Grating Polarizer to 106.4GHz ECH System on Heliotron-E

K. Nagasaki, A. Isayama and A. Ejiri

(Received - Jan. 11, 1995)

NIFS-334 Jan. 1995

RESEARCH REPORT
NIFS Series

NAGOYA, JAPAN

Application of Grating Polarizer to 106.4GHz ECH System on Heliotron-E

K. Nagasaki, A. Isayama[A] and A. Ejiri[B]

Plasma Physics Laboratory, Kyoto University, Uji, Kyoto, 611 Japan

[A] Faculty of Engineering, Kyoto University, Kyoto, 606 Japan

[B] National Institute for Fusion Science, Nagoya, 464-01 Japan

Abstract

A grating polarizer with rectangular grooves is designed for 106.4GHz electron cyclotron heating (ECH) system on the Heliotron-E helical device. The polarizer is installed on mirrors of waveguide miter bends. In oversized waveguides, the HE_{11} mode can be treated by the plane wave theory. The polarization of the reflected wave is calculated as a function of the groove parameters and the mirror rotation angle. When launching the ECH power to fusion devices with moderate or strong magnetic shear such as heliotron/torsatron configurations, we should take into account the change of the wave polarization through the plasma. The effect of the magnetic shear can be investigated by using the polarizer. The dependence of the absorbed power on the mirror rotation angle are presented.

Keywords: ECH, Heliotron-E, HE_{11} transmission line, grating polarizer, magnetic shear, launching condition

1. Introduction

Electron cyclotron heating (ECH) has been successfully utilized for fusion plasmas. Besides the plasma heating, ECH systems have been recognized as useful tools for plasma production, current drive, plasma profile modification, MHD control and transport study. So far the ECH power generated by gyrotrons has been transmitted with the TE_{01} or TE_{02} modes. However, with higher frequency, higher power and longer pulse lengths, more efficient and reliable transmission system is required. Recently the ECH transmission line has been made progress [1] [2]. Two types of transmission schemes are now under development and already partly in use. One is oversized tubular HE_{11} mode waveguide, and the other is quasi-optical TEM_{00} transmission using focusing reflectors. The former is used in Heliotron-E[3] and DIII-D[4], and the latter is used in W7-AS[5] and CHS[6].

Polarizers are required to be set up in these transmission lines in order to correct the polarization which may be changed by successive mirrors not in the same plane and to obtain the desired polarization for effective plasma heating and current drive. Such polarizers have been used for Gaussian beam propagating through free space. Universal polarizers using two or three mirrors have been proposed[7] . Combinations of smooth and grooved mirrors can give an arbitrary polarization. The groove parameters are obtained by calculating the dependence of the phase shift between the field components parallel and perpendicular to the grooves on the mirror rotation angle[8][9]. This method is also useful for the HE_{11} transmission line using oversized corrugated waveguides. The polarizers are installed on the plane mirror of the miter bend. Doane[10] has shown that his experimental results are in good agreement with the plane wave theory. Since the waveguide of 106.4GHz ECH system on Heliotron-E is oversized, $D = 63.5mm\phi$, we can apply the plane wave theory for designing the polarizer in our system.

Usually the launching conditions for ECH have been determined only by the direction of the resonant magnetic field. For extraordinary(X)-mode heating, for example, the

wave is launched so that the electric field is perpendicular to the orientation of the magnetic field at the resonance layer. However, in fusion devices with moderate or strong magnetic shear such as Heliotron-E, CHS and LHD heliotron/torsatron configurations, it has been pointed out that we should take into account the effect of the magnetic shear on the launching conditions for good single pass absorption[11]. The launched wave should be elliptically polarized even in the perpendicular launching case. Installation of the polarizer in the HE_{11} transmission line would enable us to investigate experimentally the shear effect and to find the optimum conditions for effective heating.

In this paper, the grating polarizer using the rectangularly grooved mirror is designed for 106.4GHz ECH system on Heliotron-E. The organization of the paper is as follows. In Sec.2, we briefly review the plane wave theory for rectangularly grooved mirrors. The groove parameters are determined according to the linear and circular polarization. In Sec.3, the wave propagation through the plasma is calculated by considering the effect of the sheared magnetic field. The absorbed power fraction in the single path is shown as a function of the rotation angle of the grooved mirror. Conclusions are found in Sec.4.

2. Grating Polarizer in HE_{11} Transmission Line

The geometry of the system is illustrated in Fig.1. The incident wave is linearly polarized, whose direction is determined by the angle ψ. The angles, θ and ϕ, are the spherical coordinates, and the mirror, which has rectangular grooves on its surface, is rotatable around the normal axis of the mirror by the angle Φ. The plane of incidence is perpendicular to the plane of polarizer. By the grating polarizer, the linearly polarized incident wave can be changed into the elliptically polarized reflected wave. The polarization of the reflected wave is characterized by the rotation angle, α, and the ellipticity, β, of the ellipse. At $\beta = 0°$, for example, the reflected wave is linearly polarized, and at $\beta = 45°$, it is circularly polarized.

To determine the relation between the incident and reflected waves, the incident field

is decomposed into two orthogonal modes, the fast and slow polarizations. They are also called the TE- and TM-like modes, respectively, because they become the TE and TM modes when the incident wave vector is perpendicular to the plane of the mirror ($\theta = 0°$). The magnetic field of the TM-like mode does not have a component in the groove direction, and the electric field of the TE-like mode does not have a component in the groove direction. The TE-like mode penetrates into the grooves, while the TM-like mode reflects at the surface, leading to the phase shift between them.

The relation between the incident and reflected wave is given as

$$\begin{aligned}\begin{pmatrix} E_{\theta r} \\ E_{\phi r} \end{pmatrix} &= \begin{pmatrix} \cos\xi & \sin\xi \\ -\sin\xi & \cos\xi \end{pmatrix} \begin{pmatrix} \exp(i\frac{\tau}{2}) & 0 \\ 0 & \exp(-i\frac{\tau}{2}) \end{pmatrix} \begin{pmatrix} \cos\xi & -\sin\xi \\ \sin\xi & \cos\xi \end{pmatrix} \begin{pmatrix} E_{\theta i} \\ E_{\phi i} \end{pmatrix} \\ &= E_0 \begin{pmatrix} \cos\psi & \cos(2\xi+\psi) \\ \sin\psi & -\sin(2\xi+\psi) \end{pmatrix} \begin{pmatrix} \cos\frac{\tau}{2} \\ i\sin\frac{\tau}{2} \end{pmatrix} \end{aligned} \tag{1}$$

where $E_{\theta i}$, $E_{\phi i}$ and $E_{\theta r}$, $E_{\phi r}$ are the electric field components of the incident and reflected waves, respectively. The parameter ξ is given as $\xi = \tan^{-1}(\tan\phi \cdot \cos\theta)$, and satisfies the relation $\sin\xi \cdot E_\theta + \cos\xi \cdot E_\phi = 0$ for the TM-like mode. The phase difference, τ, between the TE- and TM-like modes has the same definition as in ref.[8].

When we write the components $E_{\theta r}$ and $E_{\phi r}$ as $E_{\theta r} = E_0 \hat{E}_\theta \exp\{i(kz - \omega t + \delta_\theta)\}$, $E_{\phi r} = E_0 \hat{E}_\phi \exp\{i(kz - \omega t + \delta_\phi)\}$, then $\hat{E}_\theta$, $\hat{E}_\phi$, δ_θ and δ_ϕ are given as

$$\hat{E}_\vartheta = \sqrt{\left\{\cos\psi\cos\frac{\tau}{2}\right\}^2 + \left\{\cos(2\xi+\psi)\sin\frac{\tau}{2}\right\}^2} \tag{2}$$

$$\hat{E}_\phi = \sqrt{\left\{\sin\psi\cos\frac{\tau}{2}\right\}^2 + \left\{\sin(2\xi+\psi)\sin\frac{\tau}{2}\right\}^2} \tag{3}$$

$$\delta_\theta = \tan^{-1}\left\{\frac{\cos(2\xi+\psi)\sin\frac{\tau}{2}}{\cos\psi\cos\frac{\tau}{2}}\right\} \tag{4}$$

$$\delta_\phi = \tan^{-1}\left\{\frac{-\sin(2\xi+\psi)\sin\frac{\tau}{2}}{\sin\psi\cos\frac{\tau}{2}}\right\}. \tag{5}$$

When we define the phase shift between $E_{\theta r}$ and $E_{\phi r}$ as $\delta \equiv \delta_\theta - \delta_\phi$, then the angles, α and β, of the reflected wave are obtained by solving the following equations,

$$\left(\frac{\cos\alpha}{\cos\beta}\right)^2 + \left(\frac{\sin\alpha}{\sin\beta}\right)^2 = \left(\frac{1}{\hat{E}_\theta \sin\delta}\right)^2 \tag{6}$$

$$\left(\frac{\sin\alpha}{\cos\beta}\right)^2 + \left(\frac{\cos\alpha}{\sin\beta}\right)^2 = \left(\frac{1}{\hat{E}_\phi \sin\delta}\right)^2 \tag{7}$$

$$\sin 2\alpha\left(\frac{1}{\cos^2\beta} - \frac{1}{\sin^2\beta}\right) = -\frac{2\cos\delta}{\sin^2\delta}\frac{1}{\hat{E}_\theta}\frac{1}{\hat{E}_\phi} \tag{8}$$

where $-90° \le \alpha \le 90°$, $0° \le \beta \le 45°$, the right rotation if $\delta > 0$ and the left rotation if $\delta < 0$.

The groove is characterized by the period, p, width, w, and depth, h, as shown in Fig.2. If the groove period, p, satisfies $p < \lambda/(1+\sin\theta\cos\phi)$, then only the zeroth order mode is propagating. Here λ is the wavelength of the incident wave. For our system ($\theta = 45°$), this condtion gives $p < 0.586\lambda$. The phase shift, τ, is a function of the groove parameters, p, w, h, and the mirror rotation angle. The calculation methods for determining the phase shift, τ, have been suggested by Kok and Gallagher[12][13], and a slight modification has been made by Doane[10] in order to avoid a numerical instability. The equations for the phase shift can be found in the Appendix.

Two types of polarizer are designed in this paper. One is a linear polarizer and the other is a circular one. The rotation angle, α, and ellipticity, β, of the reflected

wave are dependent on the mirror rotation angle as shown in Fig.3. In the case of the linear polarizer (Fig.3(a)), we have the arbitrary rotation angle α. The polarization is purely linear only at $\Phi = 0°, \pm 54°$ and $\pm 90°$. However, the reflected wave may be considered to be almost linear over the mirror rotation angle, Φ, because the ellipticity is less than 10°, which also means that the power contained by the componenent in the direction of the short axis of the ellipse is less than 3%. The arbitrary rotation angle, α, is also obtained in the circular polarizer (Fig.3(b)). However, the reflected wave can be circularly polarized only around $\pm 55°$.

In Fig.4, the mirror rotation angle, Φ, to get a purely linear polarization and the resultant rotation angle, α, of the reflected wave is plotted as a function of the groove depth. The phase shift, τ, has a limited range when the groove depth is fixed. Thus the linear polarization is obtained in the range $0.26 \leq h/\lambda \leq 0.36$.

In the actual 106.4GHz ECH system on Heliotron-E, the incident wave is slightly tilted as $\psi = 98°$, and the launching angle is not perpendicular to the central magnetic field of the Heliotron-E device even without the polarizer, that is, the angle between the central magnetic field and launching angle is 17°. Considering these modifications and changing the viewing direction from $-\mathbf{k}_r$ to $\mathbf{k}_r$, we obtain the dependence of polarization parameters on the mirror rotation angle as shown in Fig.5. In the next section, the effect of magnetic shear on wave propagation is studied by using this polarizer.

3. Effect of magnetic shear on wave propagation through plasma

The 106.4GHz ECH power is launched from the top of the torus, which corresponds to low field side injection. In heliotron/torsatron configurations such as Heliotron-E, CHS and LHD, the magnetic field has moderate or strong shear, especially at the plasma boundary. Since the launched wave is coupled to the plasma at the boundary, the orientation of the magnetic field at the boundary is an important factor. It is also

known that the magnetic shear can affect the wave propagation through the plasma [15][16][17].

To analyze the magnetic shear effect, a simple slab geometry in the fixed Cartesian coordinates is used. The electron cyclotron wave propagates in the z-direction which is along the density gradient and perpendicular to the magnetic field of the system. The magnetic field is assumed to be sheared in the $x-y$ plane, and has an angle ζ with the x-axis. This assumption is appropriate in Heliotron-E, because B_z is negligibly small ($|B_z/B| \lesssim 3 \times 10^{-5}$).

The second order coupled equations for the O- and X-modes are given as[18]

$$\frac{d^2E_{\|}}{dz^2} + (\frac{\omega^2}{c^2}N_O^2 - \eta^2)E_{\|} = 2\eta\frac{dE_{\perp}}{dz} + \frac{d\eta}{dz}E_{\perp} \tag{9}$$

$$\frac{d^2E_{\perp}}{dz^2} + (\frac{\omega^2}{c^2}N_X^2 - \eta^2)E_{\perp} = -2\eta\frac{dE_{\|}}{dz} - \frac{d\eta}{dz}E_{\|} \tag{10}$$

where $E_{\|}$ and $E_{\perp}$ are the components parallel and perpendicular to the local magnetic field, N_O and N_X are the refractive indices for the O- and X-modes in a cold plasma, $N_O^2 = 1-p$, $N_X^2 = \{(1-p)^2 - q\}/(1-p-q)$, $p = \omega_p^2/\omega^2$, and $q = \omega_c^2/\omega^2$. ω_p, ω_c and ω are the plasma frequency, cyclotron frequency and frequency of the launched microwave, respectively. η is the magnetic shear defined as $\eta \equiv d\zeta/dz$. The electric field can be numerically calculated by integrating eqns.(9) and (10) along the propagation path. In this calculation, the electron cyclotron absorption is also included, because the second harmonic X-mode is strongly absorbed at the resonance layer [19].

The electric field along the propagation path (z-axis) is shown in Fig. 6. The wave with 106.4GHz frequency (the wave length $\lambda = 2.82mm$) is launched from $z = 0.4$, and the mirror rotation angle is set to be 0°. The electric field is normalized by the initial field strength. Since the electric field oscillates with a period $\lambda = 2\pi c/N\omega$, the

envelope of the oscillation is plotted. The electron density profile is assumed to be broad, $n_e(z) = n_e(0)\{1-(z/a)^6\}$, $n_e(0) = 1\times 10^{19}m^{-3}$, and the electron temperature profile is assumed to be parabolic, $T_e(z) = T_e(0)\{1-(z/a)^2\}$, $T_e(0) = 1keV$ where a is the plasma boundary radius. The plasma boundary is set to be $a = 0.3m$, which corresponds to the minor radius of the outermost magnetic surface. Without the plasma, the X- and O-modes degenerate and do not rotate with the magnetic field. Since the launched wave is tilted, $\alpha = -23.2°$, the X-mode power fraction has a maximum around $z = 0.2$. With the plasma, due to the shear effect, both modes do not propagate independently, and the envelope of the electric field oscillates along the propagation path as shown in Fig.6(a).

When the central magnetic field is lower than the second harmonic resonant field, that is, $B(0) < 1.90T$, then the resonance layer is located in the high field side (helical coil side) so that the wave does not cross the resonance layer and escapes from the plasma without absorption. Measurement of the polarization at the opposite side of the same poloidal section ($z = -0.4$ in Fig.6) should show us a strong rotation of the launched wave if the magnetic shear plays an important role in the wave propagation. When the central magnetic field is higher than the resonant field, $B(0) > 1.90T$, then the resonance layer is located in the low field side (launcher port side). The X-mode is strongly damped around the second harmonic resonance layer as shown in Fig.6(b).

Figure 7 shows the dependence of the absorbed power fraction on the mirror rotation angle. The absorbed power has maxima 90%($\Phi = -88°$), 89%($\Phi = 2°$) of the launched power, and minima 8%($\Phi = -52°$), 7%($\Phi = 58°$). The shift of the maximum and minimum positions is so large that it could be experimentally measurable.

4. Conclusion

The grating polarizer for the HE_{11} transmission line was designed for the 106.4GHz ECH system on Heliotron-E. The polarizer is placed on mirrors of miter bends. In oversized waveguides, the HE_{11} mode can be treated by plane wave theory. The relation

between the incident and reflected waves is a function of the groove parameters and the mirror rotation angle. The rectangular groove parameters of pitch, width and depth are determined for the linear and circular polarizations.

Arbitrary polarization is available if the two grating mirrors are installed in the transmission line. In our system, however, we will use only one mirror as a polarizer. One reason is that the elliticity is small over the mirror rotation angle if the groove parameters are suitably chosen. The reflected wave is nearly linear, to the extent that we should be able to investigate the magnetic shear effect on the wave propagation through the plasma. Another reason is that we can reduce the probability of an arc breakdown occurring in the transmission line. Rounding off the ribs is one of the solutions to avoid the arc breakdown, but the phase difference between the TE- and TM-like modes is changed, giving rise to a modification of the polarization of the reflected wave.

In moderate or strong magnetic shear configurations such as Heliotron-E, CHS and LHD, the O- and X-modes do not propagate independently through the plasma, and rotate with the magnetic field. The dependence of the absorbed power on the mirror rotation angle were calculated. We plan to install the grating polarizer in the HE_{11} transmission line. The polarizer will be tested at high power up to 400kW, and the magnetic shear effect and optimum launching conditions will be experimentally investigated.

Acknowledgement

One of authors (K. N.) would like to thank Drs. J. L. Doane and M. Sato for useful discussions. He also thanks Dr. B. J. Peterson for careful reading of this manuscript. They are grateful to Heliotron-E and CHS staff for continuous discussions. Encouragement by Profs. T. Obiki and A. Iiyoshi is appreciated. This work was partly supported by the Grant-in-Aid for Scientific Research of the Ministry of Education in Japan.

References

[1] W. Henle, A. Jacobs, W. Kasparek, H. Kumrić, G. A. Müller, P. G. Schüller and M. Thumm, EUR-FU/80/90-99, Commission of the European Communities (1990)

[2] W. Kasparek, Proc. 8th Joint Workshop on ECE and ECRH, Gut Ising, Germany 1992 Vol.II, p.423 (1993)

[3] K. Nagasaki, M. Sato, M. Iima, S. Kobayashi, K. Sakamoto and H. Zushi, Fusion Technology **25** (1994) 419

[4] C. Moeller, E. Callis, W. DeHope, J. Doane, R. Freeman, R. Prater, D. Remsen and L. Sevier, Proc. 18th Conf. Controlled Fusion and Plasma Physics, Berlin, 1991, Vol.III, p.369, EPS (1991)

[5] W. Henle, et al., Proc. 16th Symp. on Fusion Technology 1990 (SOFT), London, p.1142, Elsevier Science Publishers B. V. (1991)

[6] S. Kubo, et al., to be published in Fusion Eng. Design

[7] W. Kasparek, H. Kumrić, G. A. Müller, P. G. Schüller, V. Erckmann and M. Thumm, Proc. 1st Int. Workshop on ECRH Transmission Systems (Cocoa Beach, Florida, 1990)

[8] F. M. A. Smits, Proc. 7th Joint Workshop on ECE and ECRH, Hefei (1989)

[9] J. D. Hanfling, G. Jerinic and L. R. Lewis, IEEE Trans. Antennas Propag. **AP-29** (1981) 622

[10] J. L. Doane, Int. J. Infrared and Millimeter Waves **13** (1992) 1727

[11] K. Nagasaki and A. Ejiri, to be published in Nucl. Fusion

[12] Y. -L. Kok and N. C. Gallagher, J. Opt. Soc. Am. **A5** (1988) 65

[13] Y. -L. Kok, N. C. Gallagher and R. W. Ziolkowski, IEEE Trans. Antennas Propag. **37** (1989) 901

[14] K. Nagasaki, H. Zushi, M. Sato, F. Sano, K. Kondo, S. Sudo, T. Mizuuchi, S. Besshou, H. Okada, M. Iima, S. Kobayashi, K. Sakamoto and T. Obiki, Proc. 20th European Conf. Controlled Fusion and Plasma Physics, Lisbon, 1993, Part I, p.397, EPS (1993)

[15] M. Brambilla and M. Moresco, Plasma Phys. Cont. Fusion **29** (1987) 381

[16] A. Airoldi, A. Orefice and G. Ramponi, Phys. Fluids **B1** (1989) 2143

[17] G. L. Bell, R. F. Gandy and J. B. Wilgen, Nucl. Fusion **33** (1993) 875

[18] I. Fidone and G. Granata, Nucl. Fusion **11** (1971) 133

[19] M. Bornatici, R. Cano, O. De Barbieri and F. Englemann, Nucl. Fusion **23** (1983) 1153

Figure Caption

Fig. 1 Geometry of grating polarizer, incident and reflected wave.

Fig. 2 Rectangular grooves with period p, width w and depth h.

Fig. 3 Dependence of rotation angle α and ellipticity β of reflected wave on mirror rotation Φ; (a) linear polarizer ($h/\lambda = 0.32$) and (b) circular polarizer($h/\lambda = 0.20$). The groove parameters are $w/\lambda = 0.25$, $p/\lambda = 0.35$ and $\lambda = 2.82$mm. The incident wave is perpendicular to the plane of incidence ($\psi = 90°$).

Fig. 4 Mirror rotation angle Φ for purely linear polarization and resultant rotation of reflected wave as a function of groove depth, h. ψ is 98°, and the other groove parameters are the same as in Fig.3.

Fig. 5 Application of linear polarizer to 106.4GHz ECH transmission system on Heliotron-E. The groove parameters are $w/\lambda = 0.25$, $p/\lambda = 0.35$ and $h/\lambda = 0.32$.

Fig. 6 Calculation results of propagation of second harmonic electron cyclotron wave through Heliotron-E plasma. The groove parameters are the same as in Fig.3(a). The launched wave has a polarization $\alpha = -23.2°, \beta = 5.1°$ and left rotation. The central magnetic fields are (a)1.84T and (b)1.96T. The solid and dashed lines correspond to the case with and without the plasma, respectively.

Fig. 7 Dependence of absorbed power, P_{abs}, on mirror rotation angle. The groove parameters are the same as in Fig.3(a). The central magnetic field is $1.92T$. The solid and dashed lines denote the cases with and without the plasma, respectively. In the case without the plasma, the power fraction is estimated by the power reaching the resonance layer.

Fig.A1 Cartesian coodinates and rectangular grooves

Appendix

Cartesian coordinates used is illustrated in Fig.A1. The incident wave is decomposed into two orthogonal modes, TE- and TM-like modes. By matching the fields at the groove boundary, the TE- and TM-like modes after reflection can be derived.

(a) TE-like mode

Exterior to the grooves, the electric field E_z can be written as $E_z = \cos^2\phi' \cdot u(x,y,z)$. The function $u(x,y,z)$ satisfies the Helmholz equation $\nabla^2 u + k^2 u = 0$, and is expressed by the Fourier components as follows,

$$u(x,y,z) = \exp\{i(\alpha_0 x - \beta_0 y + \gamma z)\} + \sum_{n=-\infty}^{\infty} r_n \exp\{i(\alpha_n x + \beta_n y + \gamma z)\} \qquad (A.1)$$

where $\alpha_n = \alpha_0 + n2\pi/\alpha$, $\alpha_0 = k\cos\theta'\cos\phi'$, $\beta_0 = k\sin\theta'\cos\phi'$ $\beta_n = (k_2 - \alpha_n^2 - \gamma^2)^{1/2}$, $\gamma = k\sin\phi'$ and $k = \omega\sqrt{u\epsilon}$. The transformed coordinates θ' and ϕ' are given as $\theta' = \tan^{-1}(1/\cos\phi\tan\theta)$, $\phi' = \sin^{-1}(\sin\theta\sin\phi)$. The Fourier coefficient r_n is solved by matching the fields E_z and H_x at the groove boudary .

$$U_{\ell n} r_n \exp(i\beta_n h) = V_\ell, \quad (\ell = 1, \cdots, n) \qquad (A.2)$$

where

$$\begin{cases} U_{\ell n} &= \delta_{\ell n} - \dfrac{2}{wp}(i\beta_\ell)\displaystyle\sum_{m=1}^{\infty} \frac{\tan(A_m h)}{A_m} I_{\ell m} I^*_{nm} \\ V_\ell &= -\delta_{\ell 0}\exp(-i\beta_0 h) - \dfrac{2}{wp}(i\beta_0)\exp(-i\beta_0 h)\displaystyle\sum_{m=1}^{\infty} \frac{\tan(A_m h)}{A_m} I_{\ell m} I^*_{0m}, \end{cases}$$

$$I_{nm} = \int_0^c \exp(-i\alpha_n x)\sin\left(\frac{m\pi x}{c}\right)dx$$
$$= \begin{cases} \dfrac{m\pi c}{(c\alpha_n)^2-(m\pi)^2}\{(-1)^m\exp(-i\alpha_n c)-1\} & \alpha_n^2 \neq \left(\dfrac{m\pi}{c}\right)^2 \\ -\dfrac{ic}{2} & \alpha = \dfrac{m\pi}{c} \\ \dfrac{ic}{2} & \alpha = -\dfrac{m\pi}{c}, \end{cases}$$

$$I^*_{nm} = \int_0^c \exp(i\alpha_n x)\sin\left(\frac{m\pi x}{c}\right)dx$$
$$= \begin{cases} \dfrac{m\pi c}{(c\alpha_n)^2-(m\pi)^2}\{(-1)^m\exp(i\alpha_n c)-1\} & \alpha_n^2 \neq \left(\dfrac{m\pi}{c}\right)^2 \\ i\dfrac{c}{2}, & \alpha = \dfrac{m\pi}{c} \\ -i\dfrac{c}{2}, & \alpha = -\dfrac{m\pi}{c}, \end{cases}$$

$A_m = \sqrt{a^2-(m\pi/c)^2}$ $(m = 1, 2, \cdots)$ and δ_{ln} is the delta function.

(b) TM-like mode

Exterior to the grooves, the magnetic field H_z can be written as $H_z = \cos^2\phi' \cdot v(x, y, z)$. The function $v(x, y, z)$ satisfies the equation $\nabla^2 v + k^2 v = 0$, and is expressed by the Fourier components as follows,

$$v(x, y, z) = \exp\{i(\alpha_0 x - \beta_0 y + \gamma z)\} + \sum_{n=-\infty}^{\infty} s_n \exp\{i(\alpha_n x + \beta_n y + \gamma z)\} \qquad (A.3)$$

The Fourier coefficient s_n is solved by matching the fields E_x and H_z at the groove boundary.

$$X_{ln} s_n \exp(i\beta_n h) = Y_l, \quad (l = 1, \cdots, n) \tag{A.4}$$

where

$$\begin{cases} X_{ln} &= i\beta_l \delta_{ln} + \dfrac{1}{wp} \displaystyle\sum_{m=0}^{\infty} \epsilon_m B_m \tan(B_m h) J_{lm} J^*_{nm} \\ Y_l &= i\beta_0 \exp(-i\beta_0 h)\delta_{l0} - \dfrac{1}{wp} \displaystyle\sum_{m=0}^{\infty} \epsilon_m B_m \tan(B_m h) J_{lm} J^*_{0m} \exp(-i\beta_0 h), \end{cases}$$

$$\epsilon_m = \begin{cases} 2 & (m \neq 0) \\ 1 & (m = 0), \end{cases}$$

$$\begin{aligned} J_{nm} &= \int_0^c \exp(-i\alpha_n x) \cos\left(\frac{m\pi x}{c}\right) dx \\ &= \begin{cases} \dfrac{ic^2\alpha_n}{(c\alpha_n)^2 - (m\pi)^2} \{(-1)^m \exp(-i\alpha_n c) - 1\} & \alpha_n^2 \neq \left(\dfrac{m\pi}{c}\right)^2 \\ \dfrac{c}{2} & \alpha = \pm\dfrac{m\pi}{c}, \end{cases} \end{aligned}$$

$$\begin{aligned} J^*_{nm} &= \int_0^c \exp(i\alpha_n x) \cos\left(\frac{m\pi x}{c}\right) dx \\ &= \begin{cases} \dfrac{-ic^2\alpha_n}{(c\alpha_n)^2 - (m\pi)^2} \{(-1)^m \exp(i\alpha_n c) - 1\} & \alpha_n^2 \neq \left(\dfrac{m\pi}{c}\right)^2 \\ \dfrac{c}{2} & \alpha = \pm\dfrac{m\pi}{c}, \end{cases} \end{aligned}$$

and $B_m = \sqrt{a^2 - (m\pi/c)^2} \quad (m = 0, 1, 2, \cdots)$

If the groove period satisfies $p < \lambda/(1+\sin\theta\cos\phi)$, Bragg scattering is negligible and the higher order modes do not propagate in the free space. The phase shift between the incident and reflected waves is given by $\arg[r_0 \exp(2i\beta_0 h)] - \arg[-s_0 \exp(2i\beta_0 h)]$ In this paper, the phase shift τ was calculated using $m = 20, n = 10$. The relative numerical error of the phase shift was 5.1×10^{-4}.

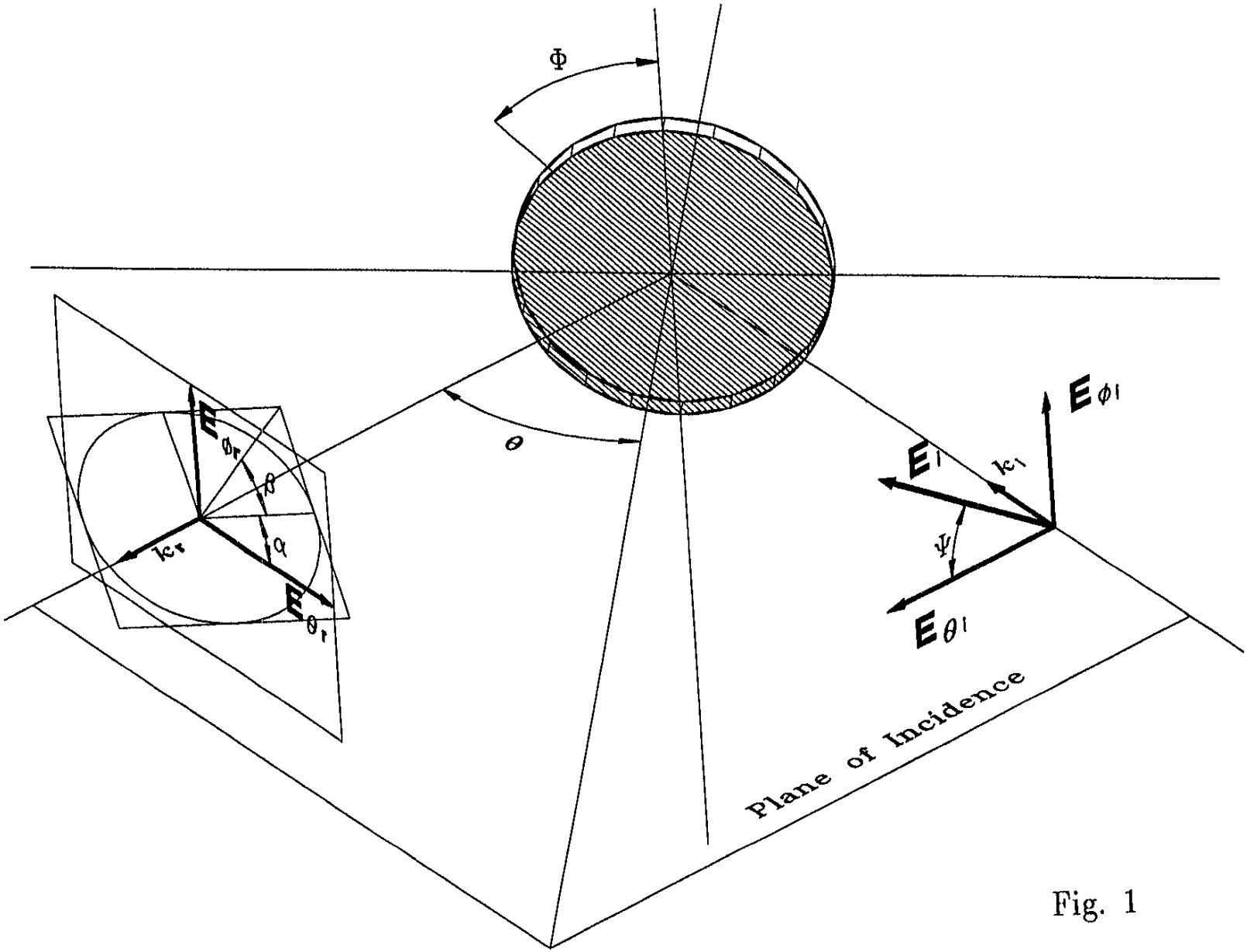
Φ
θ
$E_{\phi r}$
β
α
k_r
$E_{\theta r}$
E_i
k_i
$E_{\phi i}$
Ψ
$E_{\theta i}$
Plane of Incidence

Fig. 1

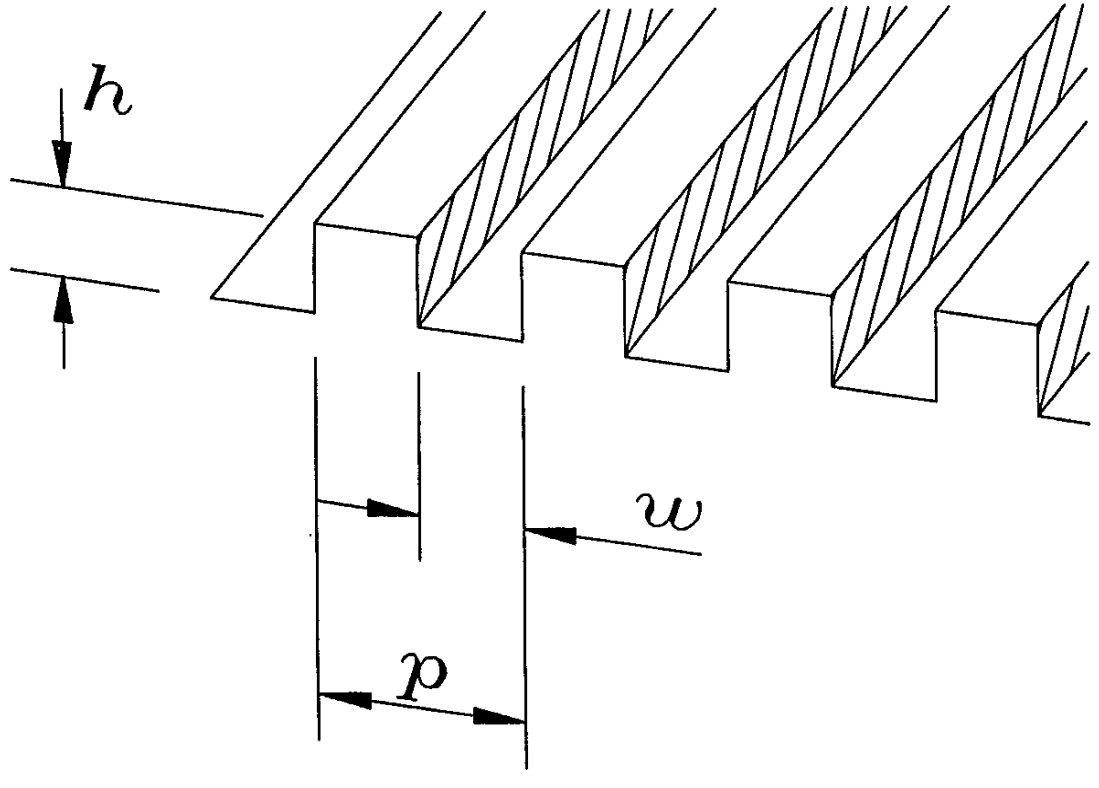

Fig. 2

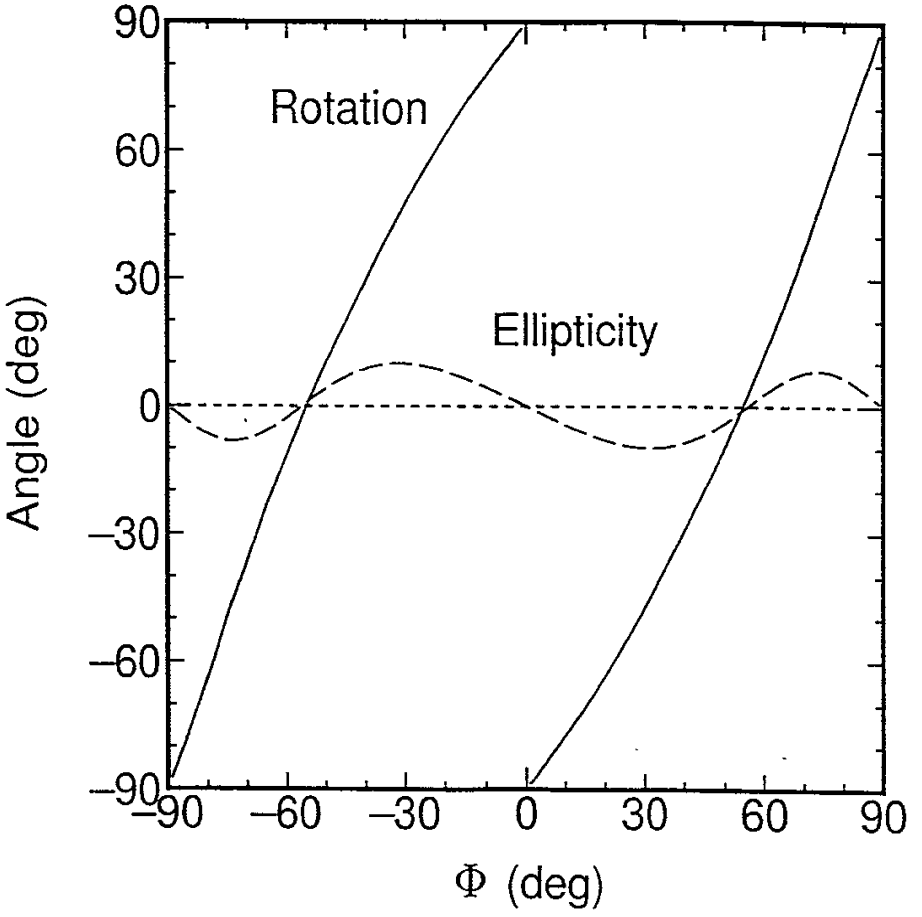
90
60
30
0
−30
−60
−90
Rotation
Ellipticity
Angle (deg)
−90
−60
−30
0
30
60
90
Φ (deg)

Fig. 3 (a)

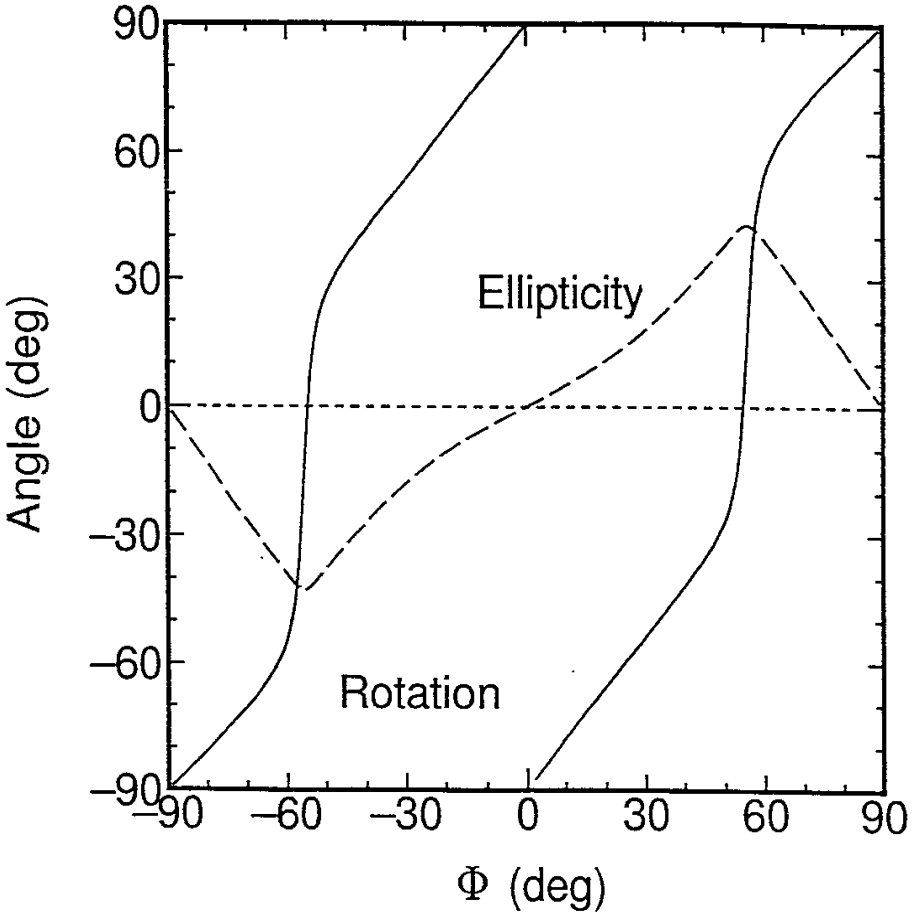
90
60
30
0
−30
−60
−90
Angle (deg)
Ellipticity
Rotation
−90
−60
−30
0
30
60
90
Φ (deg)

Fig. 3(b)

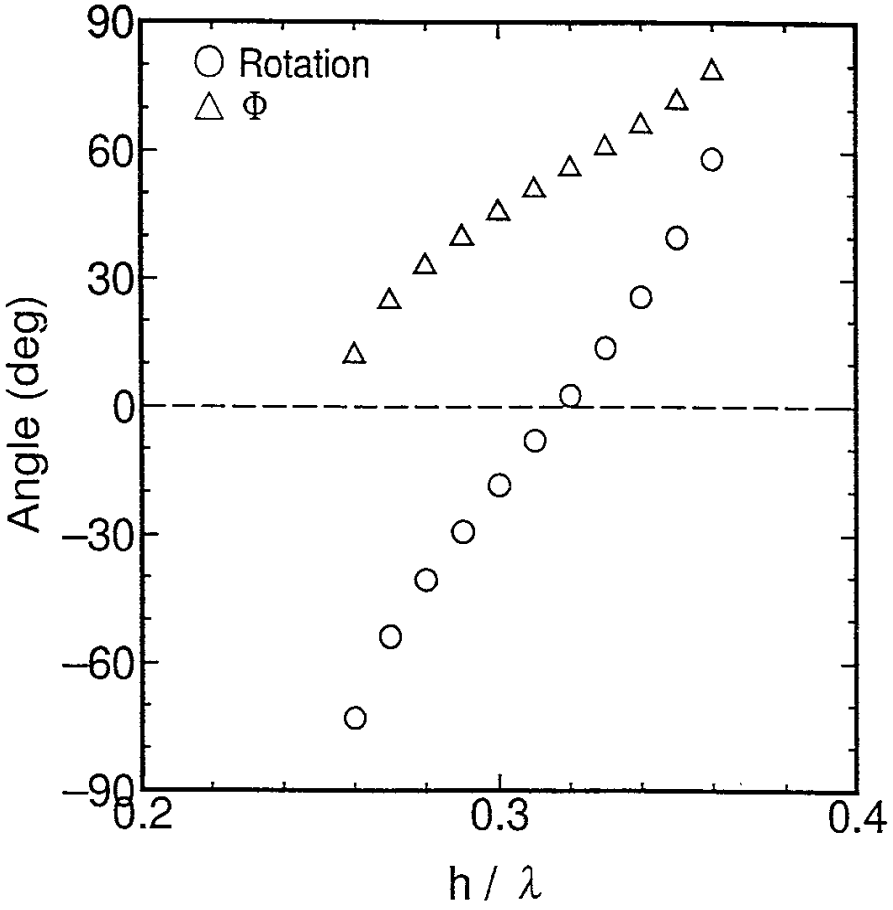

Fig. 4

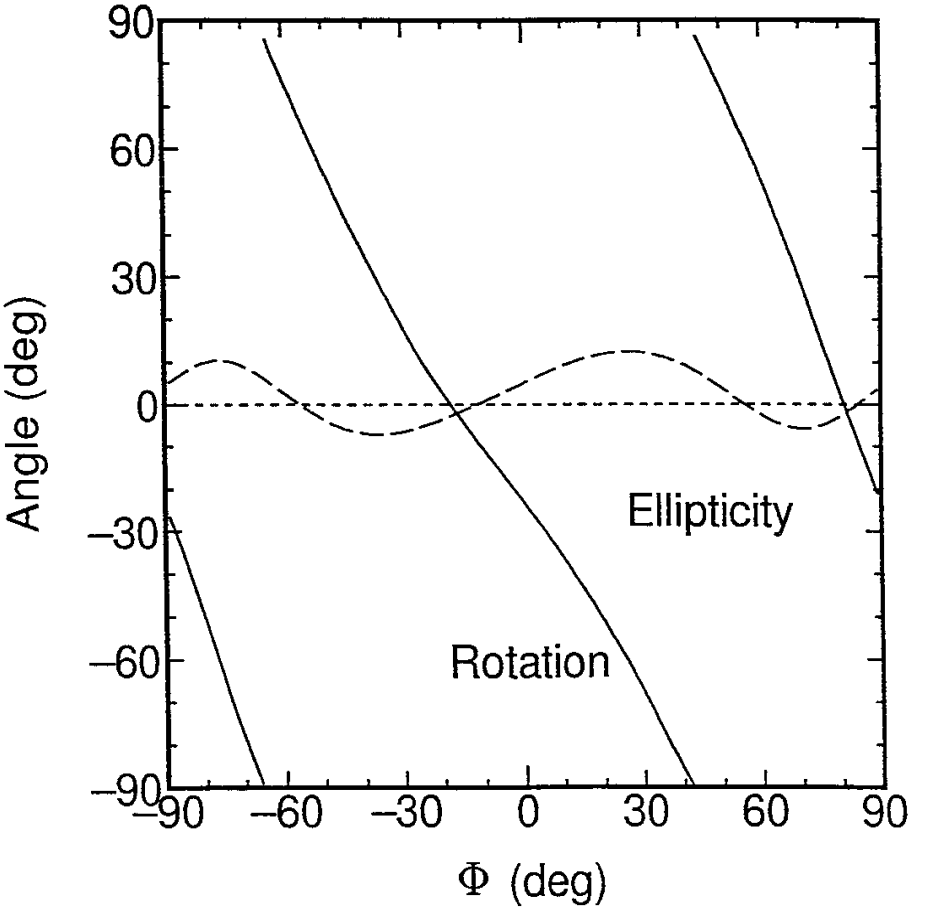
90
60
30
0
−30
−60
−90
Angle (deg)
Ellipticity
Rotation
−90
−60
−30
0
30
60
90
Φ (deg)

Fig. 5

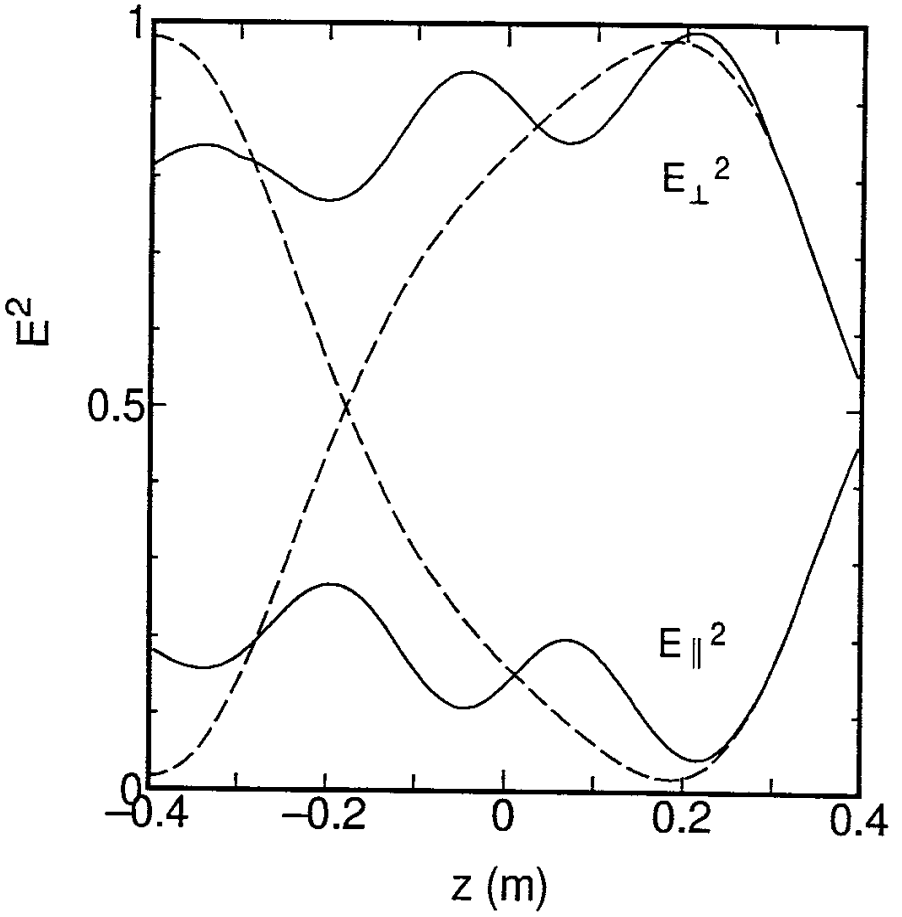

Fig. 6 (a)

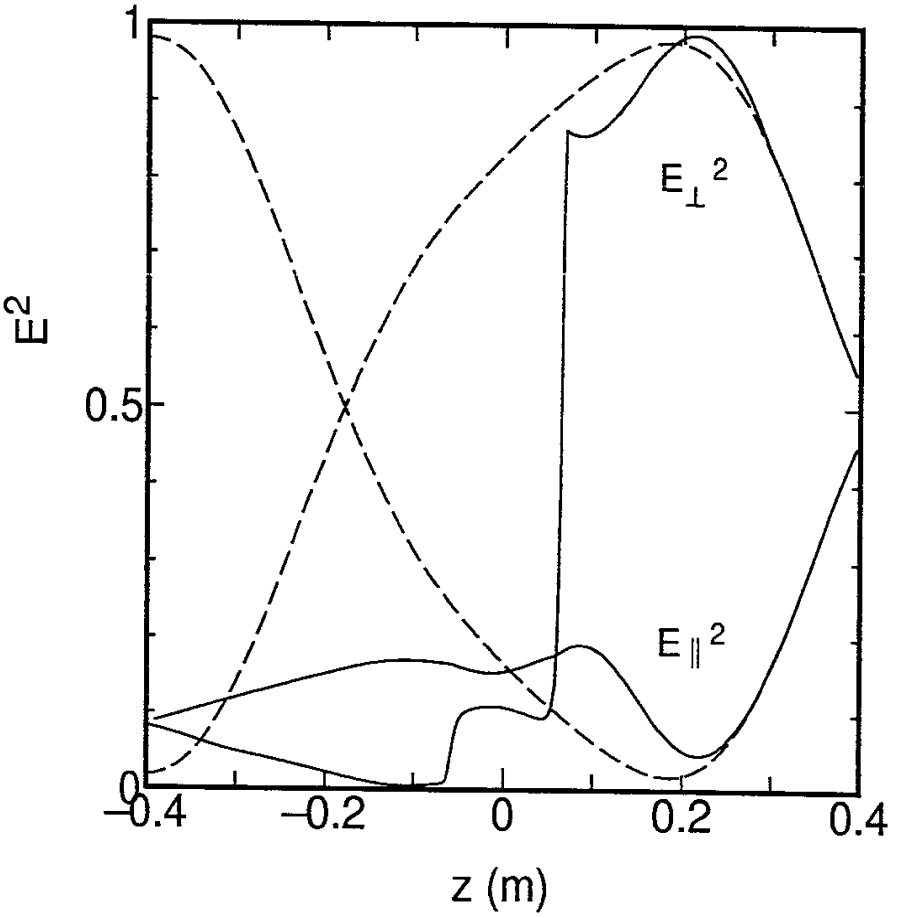

Fig. 6(b)

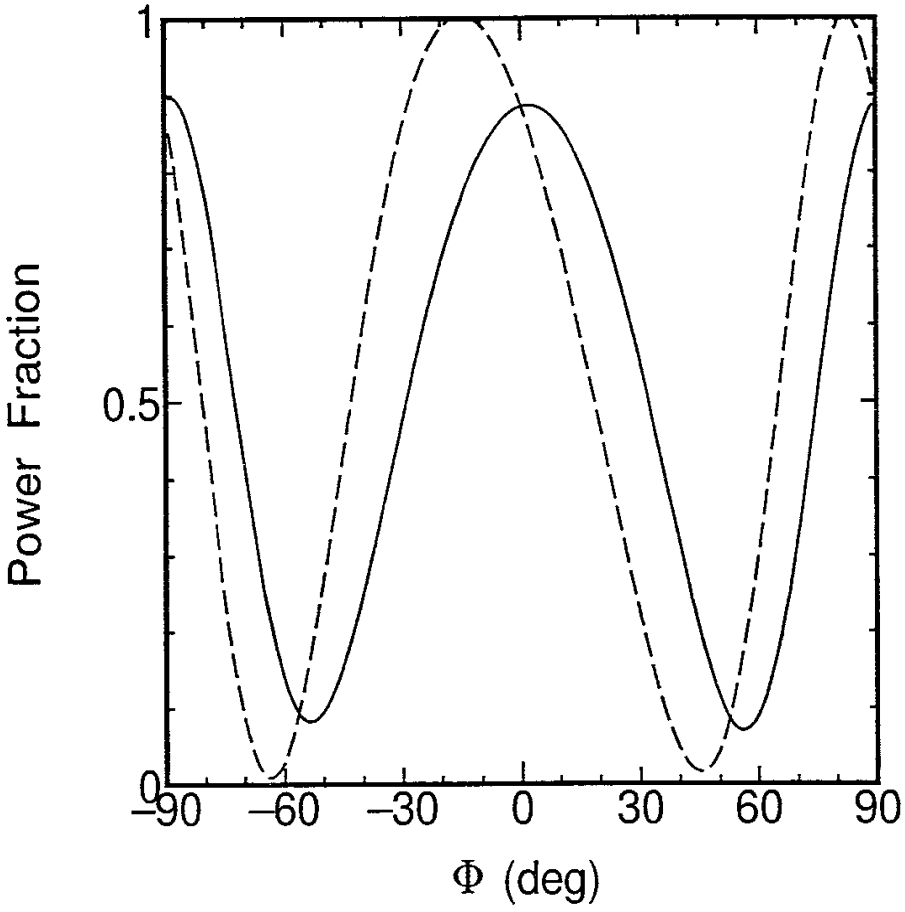

Fig. 7

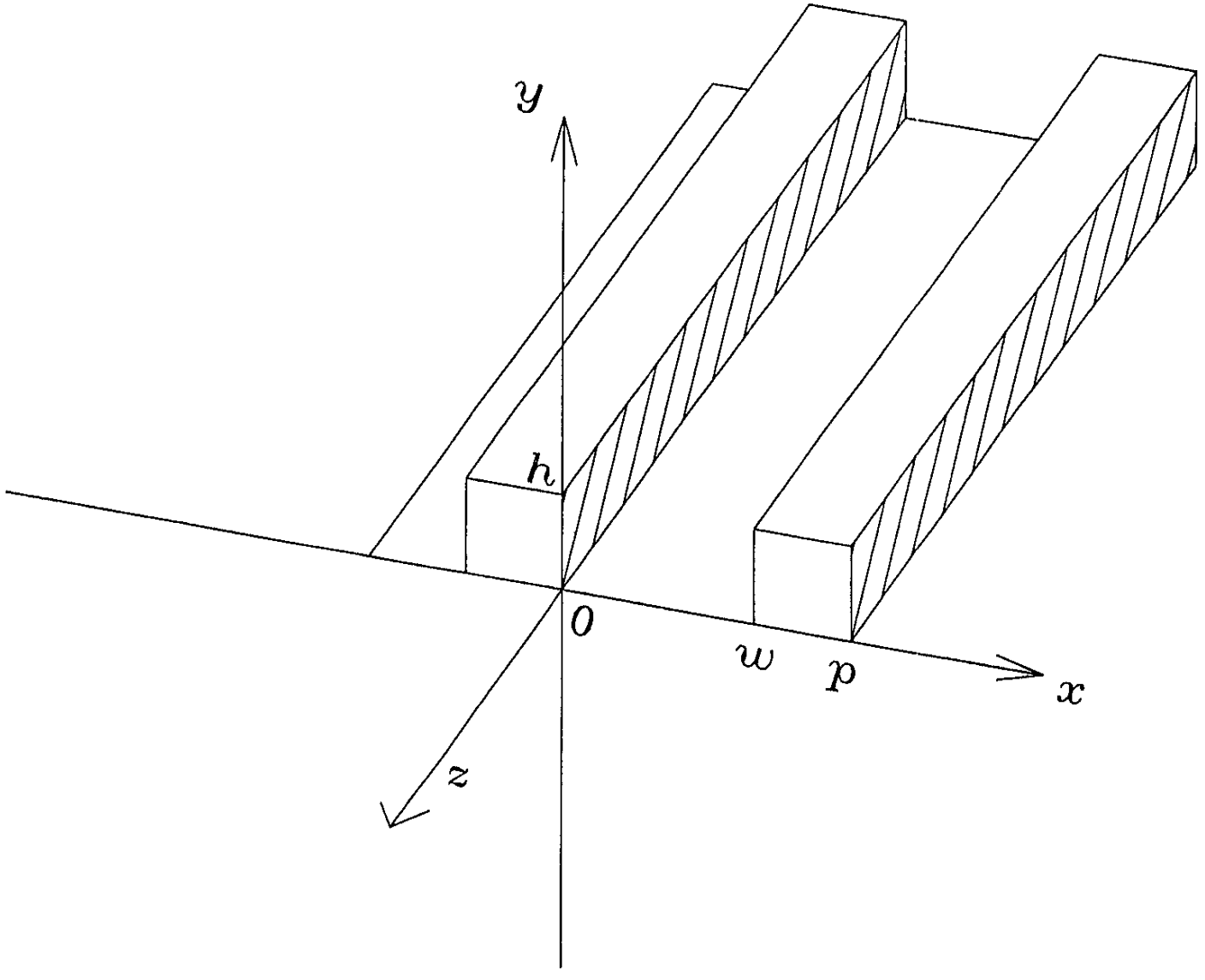

Fig.A1

Recent Issues of NIFS Series

NIFS-293 Y. Ueda, T. Tanabe, V. Philipps, L. Könen, A. Pospieszczyk, U. Samm, B. Schweer, B. Unterberg, M. Wada, N. Hawkes and N. Noda, *Effects of Impurities Released from High Z Test Limiter on Plasma Performance in TEXTOR*; July. 1994

NIFS-294 K. Akaishi, Y. Kubota, K. Ezaki and O. Motojima, *Experimental Study on Scaling Law of Outgassing Rate with A Pumping Parameter*, Aug. 1994

NIFS-295 S. Bazdenkov, T. Sato, R. Horiuchi, K. Watanabe, *Magnetic Mirror Effect as a Trigger of Collisionless Magnetic Reconnection*, Aug. 1994

NIFS-296 K. Itoh, M. Yagi, S.-I. Itoh, A. Fukuyama, H. Sanuki, M. Azumi, *Anomalous Transport Theory for Toroidal Helical Plasmas*, Aug. 1994 (IAEA-CN-60/D-III-3)

NIFS-297 J. Yamamoto, O. Motojima, T. Mito, K. Takahata, N. Yanagi, S. Yamada, H. Chikaraishi, S. Imagawa, A. Iwamoto, H. Kaneko, A. Nishimura, S. Satoh, T. Satow, H. Tamura, S. Yamaguchi, K. Yamazaki, M. Fujiwara, A. Iiyoshi and LHD group, *New Evaluation Method of Superconductor Characteristics for Realizing the Large Helical Device;* Aug. 1994 (IAEA-CN-60/F-P-3)

NIFS-298 A. Komori, N. Ohyabu, T. Watanabe, H. Suzuki, A. Sagara, N. Noda, K. Akaishi, N. Inoue, Y. Kubota, O Motojima, M. Fujiwara and A. Iiyoshi, *Local Island Divertor Concept for LHD*; Aug. 1994 (IAEA-CN-60/F-P-4)

NIFS-299 K. Toi, T. Morisaki, S. Sakakibara, A. Ejiri, H. Yamada, S. Morita, K. Tanaka, N. Nakajima, S. Okamura, H. Iguchi, K. Ida, K. Tsumori, S. Ohdachi, K. Nishimura, K. Matsuoka, J. Xu, I. Yamada, T. Minami, K. Narihara, R. Akiyama, A. Ando, H. Arimoto, A. Fujisawa, M. Fujiwara, H. Idei, O. Kaneko, K. Kawahata, A. Komori, S. Kubo, R. Kumazawa, T. Ozaki, A. Sagara, C. Takahashi, Y. Takita and T. Watari, *Impact of Rotational-Transform Profile Control on Plasma Confinement and Stability in CHS*; Aug. 1994 (IAEA-CN-60/A6/C-P-3)

NIFS-300 H. Sugama and W. Horton, *Dynamical Model of Pressure-Gradient-Driven Turbulence and Shear Flow Generation in L-H Transition;* Aug. 1994 (IAEA/CN-60/D-P-I-11)

NIFS-301 Y. Hamada, A. Nishizawa, Y. Kawasumi, K.N. Sato, H. Sakakita, R. Liang, K. Kawahata, A. Ejiri, K. Narihara, K. Sato, T. Seki, K. Toi, K. Itoh, H. Iguchi, A. Fujisawa, K. Adachi, S. Hidekuma, S. Hirokura, K. Ida, M. Kojima, J. Koog, R. Kumazawa, H. Kuramoto, T. Minami, I. Negi, S. Ohdachi, M. Sasao, T. Tsuzuki, J. Xu, I. Yamada, T. Watari, *Study of Turbulence and Plasma Potential in JIPP T-IIU Tokamak*;

Aug. 1994 (IAEA/CN-60/A-2-III-5)

NIFS-302 K. Nishimura, R. Kumazawa, T. Mutoh, T. Watari, T. Seki, A. Ando, S. Masuda, F. Shinpo, S. Murakami, S. Okamura, H. Yamada, K. Matsuoka, S. Morita, T. Ozaki, K. Ida, H. Iguchi, I. Yamada, A. Ejiri, H. Idei, S. Muto, K. Tanaka, J. Xu, R. Akiyama, H. Arimoto, M. Isobe, M. Iwase, O. Kaneko, S. Kubo, T. Kawamoto, A. Lazaros, T. Morisaki, S. Sakakibara, Y. Takita, C. Takahashi and K. Tsumori,
ICRF Heating in CHS; Sep. 1994 (IAEA-CN-60/A-6-I-4)

NIFS-303 S. Okamura, K. Matsuoka, K. Nishimura, K. Tsumori, R. Akiyama, S. Sakakibara, H. Yamada, S. Morita, T. Morisaki, N. Nakajima, K. Tanaka, J. Xu, K. Ida, H. Iguchi, A. Lazaros, T. Ozaki, H. Arimoto, A. Ejiri, M. Fujiwara, H. Idei, A. Iiyoshi, O, Kaneko, K. Kawahata, T. Kawamoto, S. Kubo, T. Kuroda, O. Motojima, V.D. Pustovitov, A. Sagara, C. Takahashi, K. Toi and I. Yamada,
High Beta Experiments in CHS; Sep. 1994 (IAEA-CN-60/A-2-IV-3)

NIFS-304 K. Ida, H. Idei, H. Sanuki, K. Itoh, J. Xu, S. Hidekuma, K. Kondo, A. Sahara, H. Zushi, S.-I. Itoh, A. Fukuyama, K. Adati, R. Akiyama, S. Bessho, A. Ejiri, A. Fujisawa, M. Fujiwara, Y. Hamada, S. Hirokura, H. Iguchi, O. Kaneko, K. Kawahata, Y. Kawasumi, M. Kojima, S. Kubo, H. Kuramoto, A. Lazaros, R. Liang, K. Matsuoka, T. Minami, T. Mizuuchi, T. Morisaki, S. Morita, K. Nagasaki, K. Narihara, K. Nishimura, A. Nishizawa, T. Obiki, H. Okada, S. Okamura, T. Ozaki, S. Sakakibara, H. Sakakita, A. Sagara, F. Sano, M. Sasao, K. Sato, K.N. Sato, T. Saeki, S. Sudo, C. Takahashi, K. Tanaka, K. Tsumori, H.Yamada, I. Yamada, Y. Takita, T. Tuzuki, K. Toi and T. Watari,
Control of Radial Electric Field in Torus Plasma; Sep. 1994
(IAEA-CN-60/A-2-IV-2)

NIFS-305 T. Hayashi, T. Sato, N. Nakajima, K. Ichiguchi, P. Merkel, J. Nührenberg, U. Schwenn, H. Gardner, A. Bhattacharjee and C.C.Hegna,
Behavior of Magnetic Islands in 3D MHD Equilibria of Helical Devices;
Sep. 1994 (IAEA-CN-60/D-2-II-4)

NIFS-306 S. Murakami, M. Okamoto, N. Nakajima, K.Y. Watanabe, T. Watari, T. Mutoh, R. Kumazawa and T. Seki,
Monte Carlo Simulation for ICRF Heating in Heliotron/Torsatrons;
Sep. 1994 (IAEA-CN-60/D-P-I-14)

NIFS-307 Y. Takeiri, A. Ando, O. Kaneko, Y. Oka, K. Tsumori, R. Akiyama, E. Asano, T. Kawamoto, T. Kuroda, M. Tanaka and H. Kawakami,
Development of an Intense Negative Hydrogen Ion Source with a Wide-Range of External Magnetic Filter Field; Sep. 1994

NIFS-308 T. Hayashi, T. Sato, H.J. Gardner and J.D. Meiss,
Evolution of Magnetic Islands in a Heliac; Sep. 1994

NIFS-309 H. Amo, T. Sato and A. Kageyama,
Intermittent Energy Bursts and Recurrent Topological Change of a Twisting Magnetic Flux Tube; Sep.1994

NIFS-310 T. Yamagishi and H. Sanuki,
Effect of Anomalous Plasma Transport on Radial Electric Field in Torsatron/Heliotron; Sep. 1994

NIFS-311 K. Watanabe, T. Sato and Y. Nakayama,
Current-profile Flattening and Hot Core Shift due to the Nonlinear Development of Resistive Kink Mode; Oct. 1994

NIFS-312 M. Salimullah, B. Dasgupta, K. Watanabe and T. Sato,
Modification and Damping of Alfvén Waves in a Magnetized Dusty Plasma; Oct. 1994

NIFS-313 K. Ida, Y. Miura, S -I. Itoh, J.V. Hofmann, A. Fukuyama, S. Hidekuma, H. Sanuki, H. Idei, H. Yamada, H. Iguchi, K. Itoh,
Physical Mechanism Determining the Radial Electric Field and its Radial Structure in a Toroidal Plasma; Oct. 1994

NIFS-314 Shao-ping Zhu, R. Horiuchi, T. Sato and The Complexity Simulation Group,
Non-Taylor Magnetohydrodynamic Self-Organization; Oct. 1994

NIFS-315 M. Tanaka,
Collisionless Magnetic Reconnection Associated with Coalescence of Flux Bundles; Nov. 1994

NIFS-316 M. Tanaka,
Macro-EM Particle Simulation Method and A Study of Collisionless Magnetic Reconnection; Nov. 1994

NIFS-317 A. Fujisawa, H. Iguchi, M. Sasao and Y. Hamada,
Second Order Focusing Property of 210° Cylindrical Energy Analyzer; Nov. 1994

NIFS-318 T. Sato and Complexity Simulation Group,
Complexity in Plasma - A Grand View of Self- Organization; Nov. 1994

NIFS-319 Y. Todo, T. Sato, K. Watanabe, T.H. Watanabe and R. Horiuchi,
MHD-Vlasov Simulation of the Toroidal Alfvén Eigenmode; Nov. 1994

NIFS-320 A. Kageyama, T. Sato and The Complexity Simulation Group,
Computer Simulation of a Magnetohydrodynamic Dynamo II: Nov. 1994

NIFS-321 A. Bhattacharjee, T. Hayashi, C.C.Hegna, N. Nakajima and T. Sato,
Theory of Pressure-induced Islands and Self-healing in Three-dimensional Toroidal Magnetohydrodynamic Equilibria; Nov. 1994

NIFS-322 A. Iiyoshi, K. Yamazaki and the LHD Group,
Recent Studies of the Large Helical Device; Nov. 1994

NIFS-323 A. Iiyoshi and K. Yamazaki,
The Next Large Helical Devices; Nov. 1994

NIFS-324 V.D. Pustovitov
Quasisymmetry Equations for Conventional Stellarators; Nov. 1994

NIFS-325 A. Taniike, M. Sasao, Y. Hamada, J. Fujita, M. Wada,
The Energy Broadening Resulting from Electron Stripping Process of a Low Energy Au^- Beam; Dec. 1994

NIFS-326 I. Viniar and S. Sudo,
New Pellet Production and Acceleration Technologies for High Speed Pellet Injection System "HIPEL" in Large Helical Device; Dec. 1994

NIFS-327 Y. Hamada, A. Nishizawa, Y. Kawasumi, K. Kawahata, K. Itoh, A. Ejiri, K. Toi, K. Narihara, K. Sato, T. Seki, H. Iguchi, A. Fujisawa, K. Adachi, S. Hidekuma, S. Hirokura, K. Ida, M. Kojima, J. Koong, R. Kumazawa, H. Kuramoto, R. Liang, T. Minami, H. Sakakita, M. Sasao, K.N. Sato, T. Tsuzuki, J. Xu, I. Yamada, T. Watari,
Fast Potential Change in Sawteeth in JIPP T-IIU Tokamak Plasmas; Dec. 1994

NIFS-328 V.D. Pustovitov,
Effect of Satellite Helical Harmonics on the Stellarator Configuration; Dec. 1994

NIFS-329 K. Itoh, S-I. Itoh and A. Fukuyama,
A Model of Sawtooth Based on the Transport Catastrophe; Dec. 1994

NIFS-330 K. Nagasaki, A. Ejiri,
Launching Conditions for Electron Cyclotron Heating in a Sheared Magnetic Field; Jan. 1995

NIFS-331 T.H. Watanabe, Y. Todo, R. Horiuchi, K. Watanabe, T. Sato,
An Advanced Electrostatic Particle Simulation Algorithm for Implicit Time Integration; Jan. 1995

NIFS-332 N. Bekki and T. Karakisawa,
Bifurcations from Periodic Solution in a Simplified Model of Two-dimensional Magnetoconvection; Jan. 1995

NIFS-333 K. Itoh, S.-I. Itoh, M. Yagi, A. Fukuyama,
Theory of Anomalous Transport in Reverse Field Pinch; Jan. 1995